Membrane Wrapping Efficiency of Elastic Nanoparticles During Endocytosis: Size and Shape Matter

Zhiqiang Shen,[†] Huilin Ye,[†] Xin Yi,[‡] and Ying Li[*,¶]

[†]*Department of Mechanical Engineering, University of Connecticut, Storrs, CT 06269, United States*

[‡]*Department of Mechanics and Engineering Science, College of Engineering, and Beijing Innovation Center for Engineering Science and Advanced Technology, Peking University, Beijing 100871, China*

[¶]*Department of Mechanical Engineering and Institute of Materials Science, University of Connecticut, Storrs, CT 06269, United States*

E-mail: yingli@engr.uconn.edu

Abstract

Using coarse-grained molecular dynamics simulations, we systematically investigate the receptor-mediated endocytosis of elastic nanoparticles (NPs) with different sizes, ranging from 25 nm to 100 nm, and shapes, including sphere-like, oblate-like and prolate-like. Simulation results provide clear evidence that the membrane wrapping efficiency of NPs during endocytosis is a result of competition between receptor diffusion kinetics and thermodynamic driving force. The receptor diffusion kinetics refer to the kinetics of receptor recruitment that are affected by the contact edge length between the NP and membrane. The thermodynamic driving force represents the amount of required free energy to drive NPs into a cell. Under volume constraint of elastic

NP, the soft spherical NPs are found to have similar contact edge lengths as rigid ones and to less efficiently be fully wrapped due to their elastic deformation. Moreover, the difference in wrapping efficiency between soft and rigid spherical NPs increases with their sizes, due to the increment of their elastic energy change. Furthermore, because of its prominent large contact edge length, the oblate ellipsoid is found to be the least sensitive geometry to the variation in NP's elasticity among the spherical, prolate and oblate shapes during the membrane wrapping. In addition, simulation results indicate that conflicting experimental observations on the efficiency of cellular uptake of elastic NPs could be caused by their different mechanical properties. Our simulations provide a detailed mechanistic understanding about the influence of NPs' size, shape and elasticity on their membrane wrapping efficiency, which serves as a rational guidance for the design of NP-based drug carriers.

KEYWORDS endocytosis, elastic nanoparticle, size, shape, wrapping efficiency

Receptor-mediated endocytosis is not only an essential process for cells to internalize molecules, macromolecules and viruses, but also a primary route exploited in drug delivery.[1–3] The ultimate goal of targeted drug delivery is to protect drug molecules and selectively deliver them to tumor sites by precisely controlling physicochemical properties (for example, size, shape, elasticity and surface chemistry) of engineered nanoparticles (NPs). Although hundreds of different NPs have been proposed and synthesized in labs, few NPs have been further used in clinical tests and approved by the US Food and Drug Administration (FDA).[4–6] Besides, most of NPs in clinical trials are spherical.[7] If we look into the nature, viruses can smartly take advantages of their elastic and geometric properties during their interaction with cells. For instance, human immunodeficiency virus (HIV) can regulate its elasticity at different life stages:[8] the immature HIV that needs to bud off the host is 14-fold stiffer than the mature HIV which becomes softer to enter the host cell. Moreover, an abundance of viral shapes persist in nature. HIV is spherical, Ebola virus is filamentous,[9] and tobacco mosaic virus exhibits a rod-like shape.[7] In comparison with the proliferation of viruses in nature, one of the important reasons leading to the gap between the huge number

of NPs in labs and their poor performance in clinical applications is the lack of mechanistic understanding of the relation between NP properties and their biological activities.

The complexity of the endocytosis process is one of the major reasons that limits our understanding. Endocytosis may refer to several different mechanisms including: macropinocytosis, clathrin-mediated endocytosis, caveolae-mediated endocytosis, calthrin/caveolae independent endocytosis and phagocytosis.[10,11] Although the specific proteins and lipids involved in these pathways are different, they share some similarities in ligand-receptor binding and membrane wrapping. Particularly, during the receptor-mediated endocytosis of engineered NPs, receptors in the cell membrane freely diffuse to encounter and bind ligands decorated on NPs. The formation of ligand-receptor bonds provides a driving force for the membrane to wrap around NPs. Therefore, both receptor diffusion kinetics and thermodynamic driving force are of great importance to determine endocytosis efficiency. On the other hand, the inconsistency of experimental conditions in different labs could be another reason that limits our understanding. Owing to large potential variables, such as NP materials, geometry, mechanical properties and cell lines, it is difficult to make a direct comparison between different experiments and draw a solid conclusion. Furthermore, these variables might be coupled together to influence the experimental results.

Despite the amount of effort that has been devoted to understanding the effects of NP's geometry on the cellular uptake process, no solid conclusions have been drawn yet,[7] and results are inconsistent between experiments. For example, Florez *et al.*[12] and Zhang *et al.*[13] reported that ellipsoidal (including oblate-like and prolate-like) NPs were easier to bind, but more difficult to be internalized by HeLa cells compared with spherical NPs. However, Sharma *et al.*[14] found that the internalization efficiency of NPs by macrophages is ranked as follows: oblate NPs $>$ spherical NPs $>$ prolate NPs. On the other hand, computational studies based on energy minimization[15,16] and molecular dynamic (MD) simulations[17,18] discovered that the oblate and prolate NPs were less favorable to be fully wrapped by the membrane than spherical NPs due to their relatively larger energy barriers. However, by

assuming the direct adhesion between the membrane and NPs during energy minimization and much larger receptor and ligand densities in MD simulations than those in biological systems, the true receptor diffusion kinetics cannot be reflected by these works. Richards *et al.*[19] considered the receptor diffusion process in theory and found that with their flat sides towards the membrane plane, oblate and prolate NPs are more efficiently wrapped by the cell membrane than their spherical counterparts. In their work, orientation of oblate and prolate NPs is fixed during the membrane wrapping process. However, this artificial orientational constraint might induce significantly unphysical effects on the energy barrier as well as the membrane wrapping efficiency for anisotropic NPs.[20–24]

The elasticity of NPs has recently attracted increasing attention for its significant role during blood circulation,[25–27] penetration in solid tumors[28,29] and tumor cellular uptake.[30,31] Nevertheless, conflicting experimental results have been reported in terms of the relation between cellular uptake efficiency and NPs' elasticity. For instance, by tuning the lipid composition in liposomes, Takechi-Haray *et al.*[28] found that liposomes with larger bending rigidity exhibited a higher rate of internalization by HeLa cells than those with smaller bending rigidity. A similar relationship was obtained by Shi *et al.*[32,33] in their investigation on the stiffness effect of core–shell poly(lactic-co-glycolic acid) (PLGA)-lipid NPs on the internalization efficiency by HeLa cells. However, by changing the layer numbers, Sun *et al.*[34] found that hyaluronic acid (HA) layer-by-layer (LBL) capsules with smaller stiffness had a higher uptake rate by HeLa cells compared to the HA LBL capsules with larger stiffness. Hartmann *et al.*[35] also found that softer polymer LBL capsules were transported to lysosomes inside HeLa cells faster than their rigid counterparts. The physical mechanisms behind these conflicting experimental results remain unknown. Both theoretical works based on the energy minimization[36,37] and MD simulations[38] found that softer NPs were energetically less favorable to be fully wrapped during the membrane wrapping process. However, as aforementioned, the conditions used in these works cannot reflect the receptor diffusion kinetics. When considering the receptor diffusion, Yi *et al.*[39] discovered that due to the larger

contact edge length, softer NPs had a larger chance to interact with the diffusive receptors. As a result, softer NPs are more efficiently fully wrapped by the cell membrane. Nevertheless, fundamental questions, such as how to relate free energy barriers to the membrane wrapping kinetics and how to relate theoretical understandings to experimental results, remain to be answered.

With these gaps between experimental results and current understanding on the influence of NPs' geometry and elasticity in mind, we developed a coarse-grained molecular dynamics (CGMD) model for elastic NPs to systematically investigate the receptor-mediated membrane wrapping of elastic NPs with different sizes and shapes. In our simulations, ligand and receptor densities are set as comparable to experimental values. The elastic NP is modeled by a thin elastic shell (Fig. 1A). Its elasticity can be systematically changed by tuning its bending constant. The settings in our simulations allow us to capture both the receptor diffusion kinetics and free energy changes during the membrane wrapping process. Our simulations provide clear evidence that the efficiency of the membrane wrapping of NPs during receptor-mediated endocytosis is a result of competition between receptor diffusion kinetics and thermodynamic driving force. The receptor diffusion kinetics refer to the kinetics of receptor recruitment that are affected by the length of the contact edge between the NP and cell membrane, as well as receptor diffusion flux. The thermodynamic driving force represents the amount of required free energy to drive NPs into the cell. Under the constraint of volume change, soft spherical NPs are found to have a similar contact edge length as their rigid counterparts. However, soft spherical NPs need to recruit more receptors to overcome larger energy barriers induced by their elastic deformation. Therefore, soft spherical NPs are less efficiently fully wrapped. Moreover, the difference in wrapping efficiency between soft and rigid NPs increases with their sizes, induced by the increment of their elastic energy change. Among spherical, oblate and prolate NPs, the oblate ellipsoid is the least sensitive geometry to the variation of NP elasticity during membrane wrapping process due to its large contact edge length. More importantly, in our simulations, both spherical and non-

spherical soft NPs remain at a high energy state when fully wrapped and cannot return to their initial stress-free state as assumed in previous theoretical studies.[36,39] In addition, simulation results indicate that the conflicting experimental observations on the efficiency of wrapping elastic NPs could be induced by the different mechanical properties of NPs. The elastic NPs with and without volume constraint can lead to inefficient and efficient cell uptake, respectively, in comparison with their rigid counterparts. Our simulations might be able to explain the conflicting experimental results and provide theoretical guidance on the rational design of NPs for targeted drug delivery.

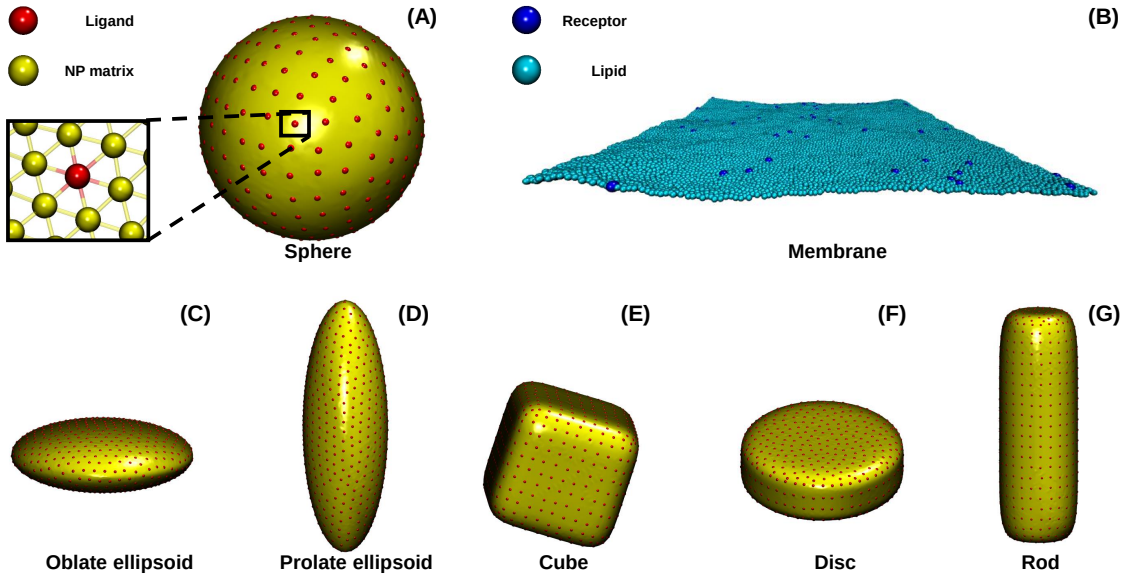

Figure 1: Computational models of elastic nanoparticles (NPs) and the cell membrane. (A) The elastic NP is represented by a thin elastic shell, which consists of interactive beads (yellow) located at the vertex points of triangles. The yellow beads are connected by harmonic bonds. The red beads represent ligands, which are evenly distributed on the NP surface. (B) A single lipid molecule is represented by one single spherical bead (colored in cyan) in our computational model. Receptors (colored in blue) in the membrane can specifically interact with ligands on the NP surface. (C-G) Models of the elastic oblate, prolate, cubic, disc-like and rod-like NPs.

Results

Internalization of Spherical Nanoparticles

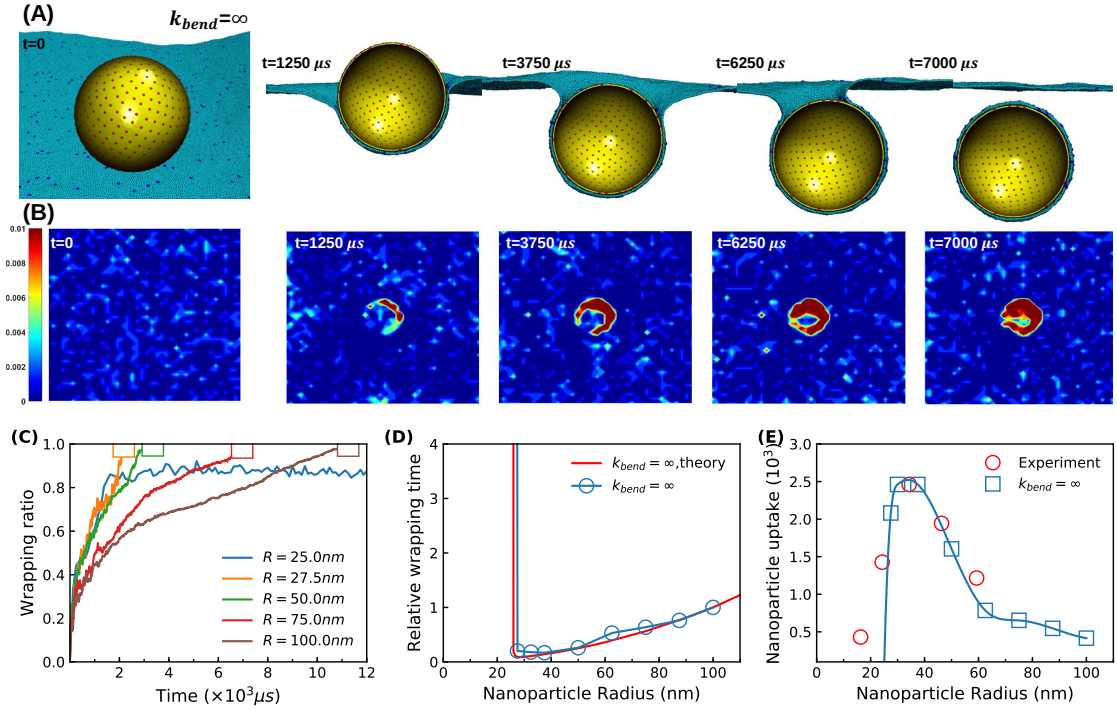

Figure 2: Membrane wrapping of rigid spherical NPs. (A) Membrane wrapping of a spherical rigid NP of radius $R = 75$ nm. (B) The receptor density distribution in the cell membrane corresponding to snapshots in (A). The color bar represents receptor density in a unit of nm^{-2}. (C) Wrapping ratio evolution at different NP radii. (D) Wrapping time as a function of the NP radius. The theoretical results for spherical rigid NPs are taken from Ref.[39] (E) Size-dependent cell uptake of rigid spherical NPs. The experimental data are taken from Ref.[40] Each simulation point in (D) and (E) is obtained by averaging five independent simulations. The error bar is small and comparable to the symbol size.

Size effect in cellular uptake of spherical rigid NPs. To correctly capture the receptor-mediated membrane wrapping process, we need to firstly confirm that our simulation model can reproduce the receptor diffusion kinetics. In terms of the receptor diffusion, a well-known phenomenon is the effect of NP size on membrane wrapping time.[39,41,42] When the size of NP is larger than its optimal value, the larger NPs need to recruit more receptors to be fully wrapped, and the diffusion of receptors to the contact region between NP and cell membrane is time consuming. Therefore, the larger NPs require more time to be fully

wrapped if their sizes exceed the optimal value.[41,43] To investigate this size effect, we firstly investigate the membrane wrapping process of rigid spherical NPs with radii ranging from 25 nm to 100 nm. The ligand density on these NPs is fixed as $9.44 \times 10^{-3}/\text{nm}^2$. The receptor density in the cell membrane is set as $6.08 \times 10^{-4}/\text{nm}^2$. Both of the densities in our model are comparable to the experimental values.[44,45] Corresponding to this low receptor density, the one-bead solvent-free lipid model[46] is adopted to provide a large membrane patch of (875×875) nm^2 (Fig. 1B). The membrane tension is controlled at zero in all simulations. The membrane bending rigidity is 24 $k_{\text{B}}T$, where k_{B} and T are the Boltzmann constant and temperature, respectively.

The snapshots in Fig. 2A show the typical membrane wrapping process of a rigid spherical NP with radius $R = 75$ nm. The spherical NP is wrapped by the membrane gradually from the bottom to top of the NP, accompanied by the bending deformation of the membrane. During this process, we inspect the receptor distribution evolution as shown in Fig. 2B. The receptors gradually aggregate in the contact region between the NP and cell membrane. Importantly, as assumed in the theory,[39,41] there exists a receptor depletion region in the near vicinity of the binding region, which is associated with the receptor diffusion flux. The membrane wrapping process and receptor distribution evolution for other sizes of rigid spherical NP are similar. The evolution of the wrapping ratio f for each spherical NP is recorded in Fig. 2C. Here f is defined as the ratio of the wrapped area to the total NP surface area. Our simulations indicate that $R = 30$ nm could be the optimum NP size with the smallest wrapping time t_w (defined as the time required for a successful NP internalization). The wrapping time for NPs of $R = 75$ nm and 100 nm is much larger than that at $R = 30$ nm. On the other hand, due to the limited ligands on the surface of the NP of $R = 25$ nm, the driving force provided by ligand-receptor binding is not large enough to overcome the energy barrier induced by the membrane bending deformation.[2] Thus, the NP of $R = 25$ nm is trapped in the membrane and cannot be fully wrapped (Fig. S2A in Supporting Information).

To compare our simulations with theoretical predictions, we normalize the wrapping time in both simulations and theory by the wrapping time of rigid NP with $R = 100$ nm in simulations and theory, respectively. As shown in Fig. 2D, our simulation results are in excellent agreement with theoretical predictions provided by Yi and Gao.[39] The choice of the reference NP size does not change the trend in these curves. Experimentally, Chithrani *et al.*[40] studied the uptake of transferrin-coated gold NPs by HeLa cells. They found that the number of NPs internalized per cell is non-monotonically dependent on the NP size. To correlate our simulation results with this experiment, we try to calculate the number N_c of NPs internalized by a cell. The N_c can be estimated as[47] $N_c = \omega N_g \Delta t_{ob}$, where $\omega = 1/t_w$ is the wrapping efficiency (wrapping rate), defined as the reciprocal of the wrapping time t_w; N_g the number of NPs adjacent to the cell; Δt_{ob} the observation time. To compare with the above experiments, we choose a value of $N_g \Delta t_{ob}$ such that the maximum uptake number N_c estimated from simulations has the same value as the one in the experiments. The results are given in Fig. 2E, where the effective size of NP R_{exp} in the experiments is shifted to $R_{exp}+9.3$ to account for the size of transferrin receptor's ectodomain.[47,48] Our simulation results again agree well with experimental results. The deviation between the simulations and experiments at $R_{exp} = 20$ nm is due to the cooperative cell uptake observed in experiments for NPs of such a small size.[40] Our computational model can reproduce and confirm the theoretical prediction[41] and experimental observation[40] on the size-dependent cell uptake of spherical rigid NPs. Moreover, the membrane wrapping process in our simulations is highly related to the internalization efficiency in experiments. In other words, our computational model can correctly capture the receptor diffusion kinetics during endocytosis, which has been ignored due to the ultra-high density of receptors in previous simulations.[49–52]

Inefficient cellular uptake of spherical elastic NPs. With the above model at hand, we further explore the influence of elasticity on the membrane wrapping of spherical NPs. Corresponding to the rigid case in Fig. 2A, the wrapping process of a soft spherical NP with $R = 75$ nm and bending constant $k_{bend} = 0.1\epsilon$ is studied first. Here k_{bend} can be directly

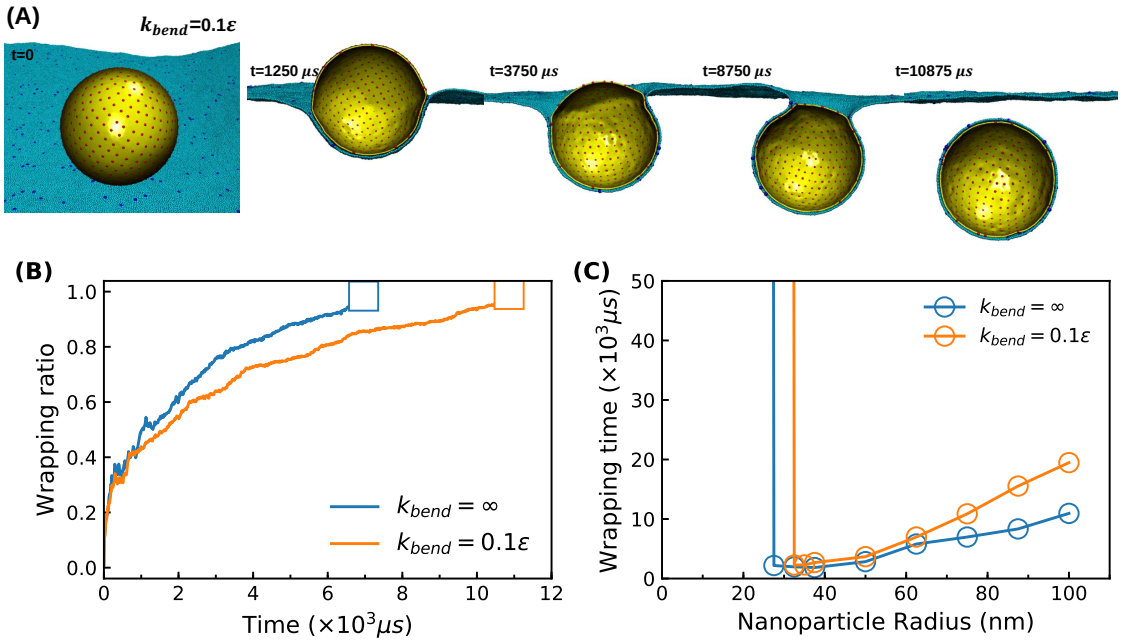

Figure 3: Membrane wrapping of soft spherical NPs. (A) Membrane wrapping of soft spherical NP with the bending constant $k_{\text{bend}} = 0.1\epsilon$ and radius $R = 75$ nm. (B) Wrapping ratio evolution for rigid ($k_{\text{bend}} = \infty$) and soft ($k_{\text{bend}} = 0.1\epsilon$) spherical NPs with identical radii $R = 75$ nm. (C) Wrapping time for rigid and soft spherical NPs of different radii.

mapped to the macroscopic bending rigidity of a soft NP.[53–55] As shown in Fig. 3A, the soft NP deforms during the wrapping process. The mean curvature at the contact edge between the wrapped and unwrapped regions is significantly increased (see Fig. S4 in Supporting Information). As the wrapping ratio increases, the contact edge moves gradually to the top of the NP, and eventually the soft NP is fully wrapped at the time $t = 10875$ μs. As shown in Fig. 3B, the soft NP is much slower to be fully wrapped than the rigid NP. To further explore the interplay between the size and elasticity of spherical NPs, we systematically investigate soft NPs ($k_{\text{bend}} = 0.1\epsilon$) of different radii and compare them with rigid NPs in Fig. 3C. There are two key phenomena we can observe from this comparison. First, the minimum size of spherical NPs that can be fully wrapped by the cell membrane is increased to $R = 30$ nm for soft NPs compared to $R = 27.5$ nm for rigid spherical NPs (cf. Fig. S2C in Supporting Information). This shift of limited size boundary is in agreement with the theoretical prediction[39] due to an additional energy barrier induced by the deformation of

soft NP. Second, all soft NPs are less efficiently wrapped than rigid ones, and the difference between them increases as the NP radius increases. It is noteworthy that this trend in our simulations seems to conflict with the theory,[39] where the soft NPs are predicted to be more efficient. The reason for this will be discussed in the following parts.

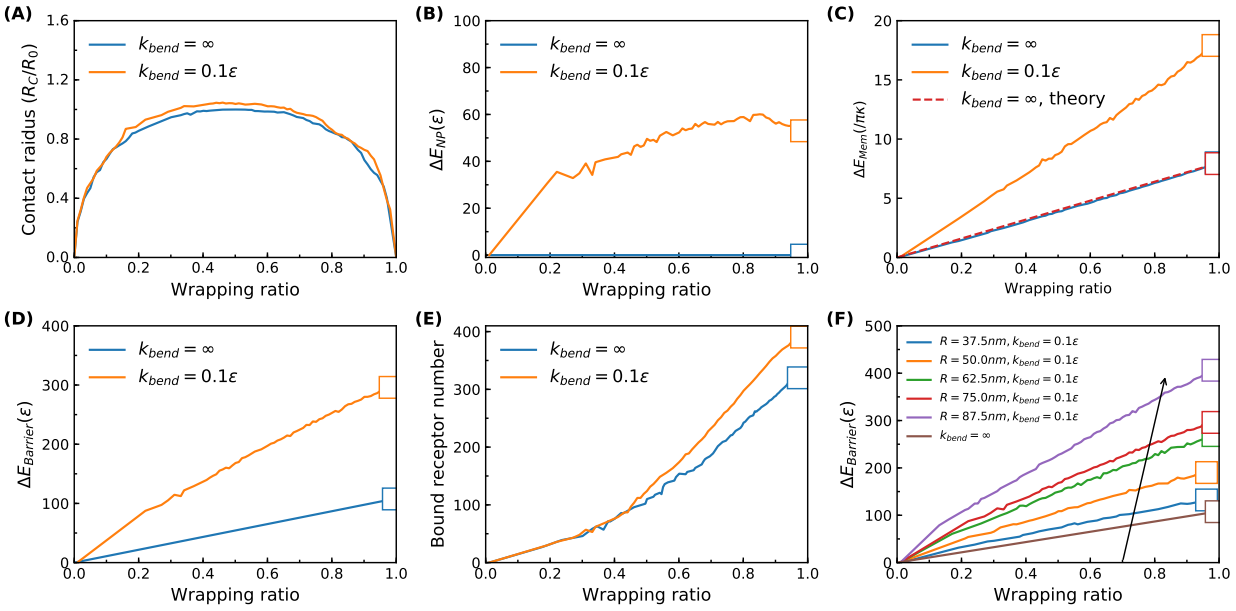

Figure 4: Free energy analysis of membrane wrapping process for spherical NPs. Comparison of (A) contact radius, (B) NP elastic energy change, (C) membrane energy change, (D) energy barrier change and (E) bound receptor numbers between rigid and soft ($k_{\text{bend}} = 0.1\epsilon$) spherical NPs at $R = 75$ nm. (F) Comparison of the energy barrier change between soft NPs with different radii.

Large energy barrier leads to inefficient wrapping of elastic NPs. As we described above, the receptor-mediated membrane wrapping process can be divided into two sub-steps: (1) the receptors diffuse to contact region between the NP and cell membrane and encounter ligands on the NP surface; (2) the binding of ligands and receptors to overcome the energy barrier induced by the membrane wrapping. The first step is a pure diffusion limited process that is related to the receptor recruiting speed. This recruiting speed is determined by the receptor diffusion flux and the length of the contact edge between the membrane and NP. The second step is a thermodynamic process that is driven by ligand-receptor binding. The number of receptors needed to achieve a certain wrapping ratio is determined by the

binding strength of individual ligand-receptor bonds and the corresponding free energy barriers. The wrapping time t_{w} depends on both the receptor recruiting speed and the number of receptors required to form ligand-receptor bonds. Therefore, the wrapping efficiency (or wrapping rate) is the result of competition between the kinetics of receptor recruitment and the amount of required driving force. In this part, we will analyze the difference between rigid and soft spherical NPs in these two aspects. In our simulations, the receptor diffusion flux is the same for all cases with fixed ligand density on the NP surface and initial receptor density in the membrane.[22,39] To estimate the contact edge length, we calculate the minimum contact circular radius in the membrane plane that can enclose the interface between wrapped and unwrapped regions of a NP. As shown in Fig. 4A, the contact radius R_{C} of a rigid spherical NP of radius $R_0 = 75$ nm firstly increases to its radius value and then decreases to zero as the wrapping ratio increases. Moreover, the contact radius of the soft NP is almost the same as that of the rigid NP at each wrapping ratio. Therefore, the receptor recruiting speed should not be the reason for the slower membrane wrapping progress of soft NPs.

The average individual ligand-receptor binding strength in our simulations is around 10ϵ. The increment of the wrapping ratio f is associated with overcoming of the corresponding energy barriers induced by the interplay among the NP, membrane and receptors. The total energy barrier $\Delta E_{\mathrm{Barrier}}$ during the membrane wrapping process is composed of three parts: (1) NP's elastic energy change ΔE_{NP}; (2) membrane energy change ΔE_{Mem}; (3) the entropy loss of receptors. Compared to the first two parts, the receptor entropy loss is negligible.[2,56,57]

The elastic energy change of a rigid NP is zero at all wrapping stages. As we demonstrated in our previous work,[51] the elastic energy change of a soft NP ΔE_{NP} is induced by the variations in its area, volume and curvature. These contributions to the energy change can be recorded in our computational model. As shown in Fig. 4B, ΔE_{NP} of a soft NP increases with the increment of the wrapping ratio until $f = 0.8$, after which it decreases slightly, ending with a value around 50ϵ at $f = 1$. Note that the elastic energy change of a soft NP is

not zero when fully wrapped. Particularly, as shown in Fig. S5 of Supporting Information, the surface area of a soft NP varies during the membrane wrapping process, and its volume is slightly decreasing. Additionally, the mean curvature distribution of the soft NP at $f = 1$ is not uniform as the initial stage as shown in Fig. S4 of Supporting Information. These results suggest that the soft NP can not return to its initial stress-free state at the full wrapping stage $f = 1$. The deformed non-spherical shape of soft NPs is maintained and stable till the end of our simulations, once they are enclosed by the cell membrane. We would like to emphasize that this non-zero energy state for fully wrapped soft spherical NPs is quite different from the stress-free state assumed in the previous theoretical works.[36,39] This non-zero energy state can be further understood by comparing to a vesicle adhering on a planar cell membrane. The in-plane stress in the contact region between vesicle and membrane is compressive.[58,59] It suggests that the wrapped region of a soft NP should be always under compression before fully wrapped. Thus, it is reasonable that the soft NP is under compression and stays at a non-zero energy state after being fully wrapped, which can be stabilized by the ligand-receptor binding.

For a membrane at zero tension, its bending energy far away from the contact region with the NP is zero, following the minimal catenoid shape surface.[23,60,61] Therefore, the membrane energy change in our simulations is only contributed to by the bending energy increment. This membrane bending calculation is non-trivial in simulations. Due to the large degrees of freedom and thermal fluctuation, the membrane energy directly recorded in the simulations has large variations and is not useful. Therefore, third party methods, such as membrane configuration estimation through theory[62–64] and a force-directed free energy calculation,[17,65] are usually applied. However, these methods might not be effective for soft NPs as it is difficult to obtain a soft NP in theoretical analysis that shares the exact same mechanical properties as the one in simulations. On the other hand, the guiding force during free energy calculation might cause additional unrelated deformations for soft NPs. Here we use another approach to compute the membrane bending energy. The membrane

in the contact region adheres to the NP surface, and they share the same curvature, as we show in the snapshots (Figs. 2 and 3). Therefore, we can utilize the configuration in the wrapped part of a NP to calculate the corresponding membrane bending energy,[23,39] particularly, based on the triangulation information.[54,55] As shown in Fig. 4C, this method can correctly capture the membrane bending energy. The membrane bending energy ΔE_{Mem} for the rigid NP linearly increases with the wrapping ratio f and reaches a value $8\pi\kappa$ at the fully wrapped stage ($f = 1$), in accord with theoretical prediction.[66] Here κ is the membrane bending modulus. In comparison, the ΔE_{Mem} for the soft NP is also linearly proportional to f, but ends with a value around $17\pi\kappa$ as the soft NP at $f = 1$ stays at a non-perfect spherical shape. Please refer to the Supporting Information for details about the membrane energy calculation.

The total energy barriers $\Delta E_{\mathrm{Barrier}}$ of rigid and soft NPs are given in Fig. 4D with $\Delta E_{\mathrm{Barrier}}$ of soft NP much larger than that of rigid NP at each f. Therefore, the soft NP needs to recruit more receptors to overcome a larger energy barrier at each stage after $f = 0.4$ (Fig. 3B). Due to the similar receptor recruiting speed as we mentioned above, the soft NP needs to wait longer than the rigid NP to encounter and bind extra receptors. That is also the reason that the soft NP is slower to be fully wrapped (cf. Fig.3B). We further calculate energy barriers of soft NPs with different sizes in Fig.4F. It is found that the energy barrier of a soft NP is increasing with the increment of the NP size. In comparison, the energy barriers of rigid NPs with different sizes are the same. This can explain how the wrapping time difference between rigid and soft NPs is increasing with their radii, as shown in Fig. 3C. In summary because of their similar contact edge length and larger energy barriers in membrane wrapping, soft spherical NPs require more time to be fully wrapped than their rigid counterparts.

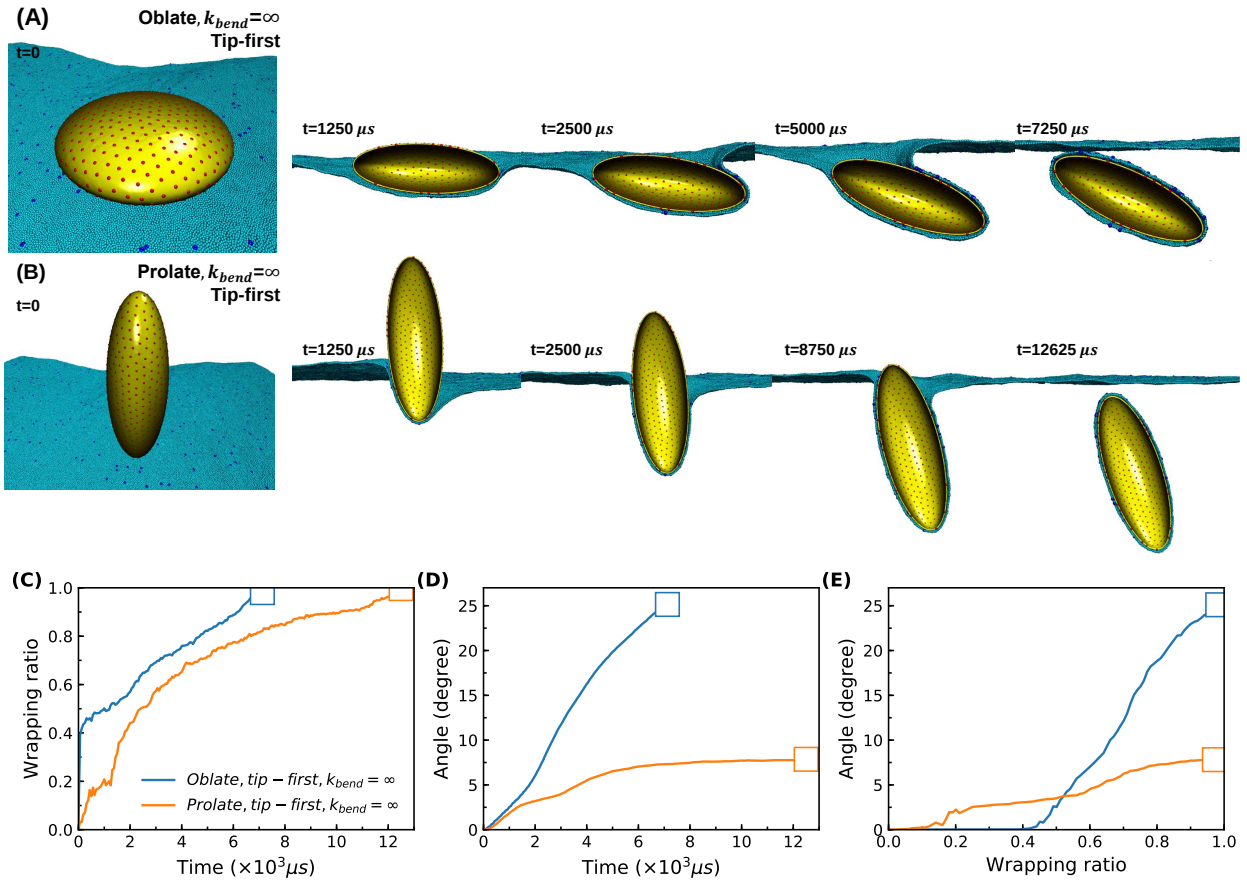

Figure 5: Membrane wrapping of rigid oblate and prolate NPs. (A-B) Snapshots of membrane wrapping process of rigid oblate and prolate NPs. (C-D) Wrapping ratio and orientation angle evolution for rigid oblate and prolate NPs. (E) Functions of orientation angle against the wrapping ratio for rigid oblate and prolate NPs.

Internalization of Nonspherical Nanoparticles

Large contact edge length results in fast internalization of oblate rigid NPs. We proceed to investigate the membrane wrapping process of rigid oblate and prolate NPs. Their initial configurations are generated based on the function $(x^2 + y^2)/a^2 + (z/b)^2 = 1$. The surface areas of both oblate and prolate NPs are controlled at the same value as the spherical NP of radius $R = 75$ nm. The aspect ratios b/a are set as $1/3$ and 3 for oblate and prolate NPs, respectively. Initially, the oblate and prolate NPs are placed above the membrane with their minor and major axes perpendicular to the membrane plane, respectively. Note that the oblate and prolate NPs are symmetric in the membrane plane. We call this entry angle

as the tip-first entry mode for the oblate and prolate NPs.

As shown in Fig.5, the membrane wrapping process for the rigid oblate NP can be divided into three different stages. In the first stage ($t < 500$ μs), due to the large contact area, half of the oblate NP is immediately wrapped by the membrane, and the wrapping ratio quickly increases to $f = 0.4$ (Fig. 5C). In the second stage (500 $\mu s < t < 2000$ μs), f increases slowly because of the highly curved edge of the oblate NP, which simultaneously rotates slowly to adjust its orientation with respect to the membrane (Fig. 5D). In the third stage ($t > 2000$ μs), one side of the oblate NP edge starts to be wrapped by the membrane. At the same time, the wrapping ratio and orientation angle begin to increase at a faster rate than in the second stage. The oblate NP is fully wrapped at $t = 7250$ μs (Fig. 5A). Compared to the oblate NP, the prolate NP is gradually wrapped by the membrane (Fig. 5B) with a slower wrapping rate than that of the oblate NP during the entire wrapping process (Fig. 5C). This result in our simulations seems to conflict with the theory that the prolate NP is more energetically favorable to be wrapped than the oblate NP with reciprocal aspect ratio.[15] Additionally, the prolate NP just slightly changes its orientation before $t = 6000$ μs ($f = 0.8$) (cf. Fig.5D), and is almost perpendicular to the membrane during the whole process. In Fig.5E, we obtain the function of orientation angle against wrapping ratio for both oblate and prolate NPs. For the oblate NP, its orientation angle would not change until $f = 0.4$, after which the orientation angle increases dramatically to 25°. This orientation variation feature of wrapping oblate NP in our simulations is consistent with the theory that can capture the orientation kinetics of ellipsoidal NPs.[22] For the prolate NP, its small orientation variation in our simulations is consistent with the theory that at zero membrane tension, one-dimensional NPs prefer a perpendicular entry angle.[22,60,67]

A key question we need to answer for the rigid oblate and prolate NP with reciprocal aspect ratios is why the energetically unfavorable oblate NP is more efficiently wrapped by the membrane than the prolate NP. We further analyze the corresponding contact edge length and energy barrier as we did for the spherical NPs. For easier comparison, the contact radii

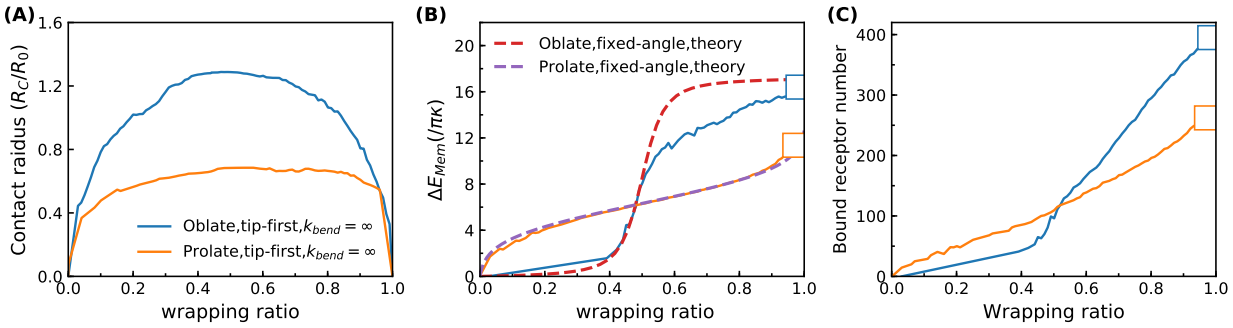

Figure 6: Free energy analysis for the membrane wrapping of rigid oblate and prolate NPs. Comparison of (A) contact edge length, (B) membrane energy barrier, and (C) bound receptor number between rigid oblate and prolate NPs. The dashed curves in (B) are obtained from the membrane energy by wrapping the same NPs but at a fixed entry angle in theory. See Fig. S6 in Supporting Information for more details.

of the oblate and prolate NPs are divided by the corresponding spherical radius $R_0 = 75$ nm. As shown in Fig. 6A, the contact radius of the oblate NP is significantly larger than that of the prolate NP between $f = 0.1$ and 0.9. This means that the oblate NP has a much larger chance to encounter receptors, which provides a higher receptor recruiting speed. On the other hand, as predicted in the theory,[15] the oblate NP needs to overcome a larger membrane energy barrier than the prolate NP after the wrapping ratio of $f = 0.5$. Correspondingly, the oblate NP needs to recruit more receptors as $f > 0.5$ (Fig. 6C). As a conclusion, though the oblate NP needs to overcome a larger energy barrier than the prolate NP during the membrane wrapping process, the oblate NP is still more efficiently fully wrapped as it has a significantly larger contact edge length. In addition, we compare the membrane energy barrier with the one having fixed entry angle in theory. As shown in Fig.6B, the orientation adjustment of the oblate NP in simulations after $f = 0.4$ is driven by the lower membrane energy barrier. While the membrane energy barrier of the prolate NP is almost the same as the one in theory with a fixed angle. Please refer to Fig. S6 in Supporting Information for details of theoretical calculation.

Interplay between geometry and elasticity in cellular uptake of nonspherical elastic NPs. We further investigate the wrapping of soft oblate and prolate NPs with the same initial configurations as rigid ones. The bending constant for both oblate and prolate

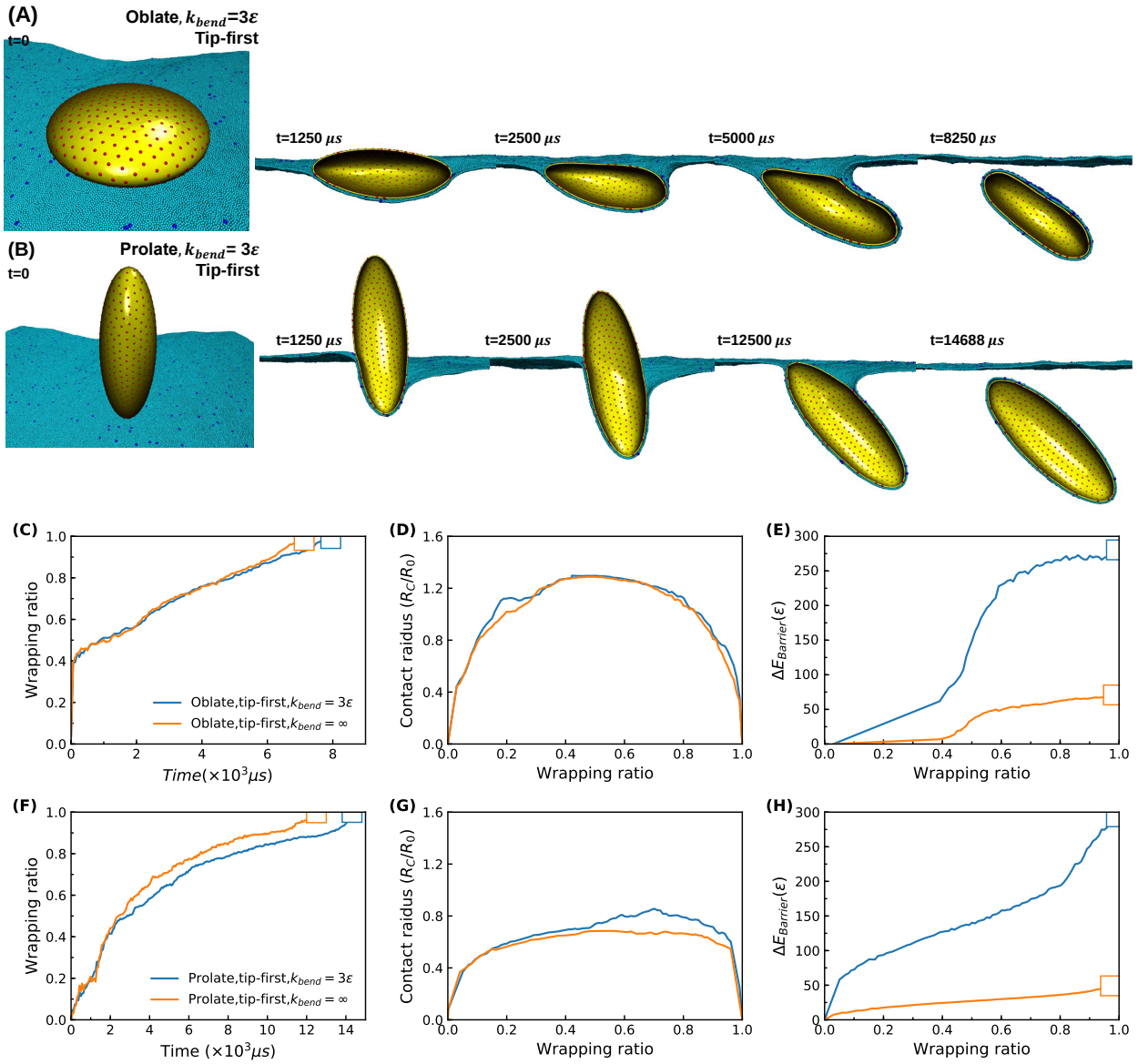

Figure 7: Membrane wrapping of oblate and prolate soft NPs with the bending constant $k_{\text{bend}} = 3\epsilon$. Membrane wrapping process of an oblate (A) and a prolate (B) soft NP. (C-E) Comparisons of the wrapping ratio, contact radius and energy barrier for rigid and soft oblate NPs. (F-H) Comparisons of the wrapping ratio, contact radius and energy barrier for rigid and soft prolate NPs.

NPs in this part is $k_{\text{bend}} = 3\epsilon$. Both soft oblate and prolate NPs follow the similar wrapping pathways as their rigid counterparts. As shown in Fig. 7A, the soft oblate NP deforms significantly near the contact edge between the NP and membrane. Specifically, its mean curvature distribution in Fig. S7 of Supporting Information indicates that the contact edge

has a large mean curvature value. Moreover, the mean curvature of the highly curved edges of soft NPs firstly increases and then decreases until fully wrapped. As shown in Fig. 7 C-E for the comparison between soft and rigid oblate NPs, it is interesting to find that their wrapping ratio evolutions are almost the same before $f = 0.9$. After that, the soft oblate NP undergoes a slower wrapping. Additionally, the contact radii of soft and rigid NPs are similar at all wrapping ratios (Fig. 7D). However, the energy barrier of the soft oblate NP is much larger than that of the rigid NP (Fig. 7E). Particularly, accompanying with the deformation, its energy barrier quickly increases to 275ϵ after $f = 0.4$. For the soft prolate NP, it also deforms and has a large mean curvature at the contact edge (Fig. 7B and Fig. S7B of Supporting Information). As shown in Fig. 7F, the wrapping of the soft prolate NP is slower than that of the rigid NP after $f = 0.4$. Similar to the oblate NPs, the evolution of the contact radii for soft and rigid prolate NPs are almost the same (Fig. 7G). The soft prolate NP needs to overcome a larger energy barrier during wrapping than the rigid one, and this energy barrier dramatically increases after $f = 0.8$, reaching 300ϵ at the end. Moreover, the energy barriers values in the wrapping process of soft prolate and oblate NPs are on the same order (around 300ϵ). Important to note is that the non-zero energy states of fully wrapped oblate and prolate NPs suggest that soft nonspherical NPs also cannot return to their initial stress-free states. It is also interesting to see that the deformation of soft NPs promotes the orientation change for both oblate and prolate NPs (Fig. S8 of Supporting Information). Please refer to the Supporting Information for details about mean curvature and orientation change during membrane wrapping process of oblate and prolate NPs.

One question we have is why the energy barrier increment during the wrapping of the soft oblate NP is not reflected on its wrapping efficiency before $f = 0.9$. We speculate that it might be related to the difference in the contact edge lengths between oblate and prolate NPs. For the oblate NPs, between $f = 0.4$ and 0.9, the minimum contact radius R_C/R_0 is 0.8. The receptor recruiting speed of oblate NP is large enough to recruit extra receptors to overcome the corresponding energy barrier increment before $f = 0.9$. After

$f = 0.9$, the contact radius quickly decreases to 0. Therefore, the membrane wrapping is sensitive to the energy barrier increment. The soft oblate NP needs to wait a longer time to recruit extra receptors, and the evolution of its wrapping ratio becomes slower than the rigid one. In comparison, for the prolate NPs, the maximum contact radius R_C/R_0 during the entire membrane wrapping process is 0.8. Given the similar energy barrier increment as soft oblate NPs, the energy barrier dominates the membrane wrapping process for prolate NPs. Thus, the prolate NP is more sensitive to this energy barrier increment during the entire wrapping process. In short, the energy barrier increment of soft NPs has different effects on the wrapping process of oblate and prolate NPs. Owing to the large contact edge length of oblate NPs, their wrapping efficiency is not sensitive to the increment of energy barrier in the first wrapping stage, while the wrapping of soft oblate NP only slows down in the late stage. In comparison, for the prolate NPs, because of their much smaller contact edge length, the wrapping process of soft prolate NPs would be more sensitive to the increment of the energy barrier during the whole process.

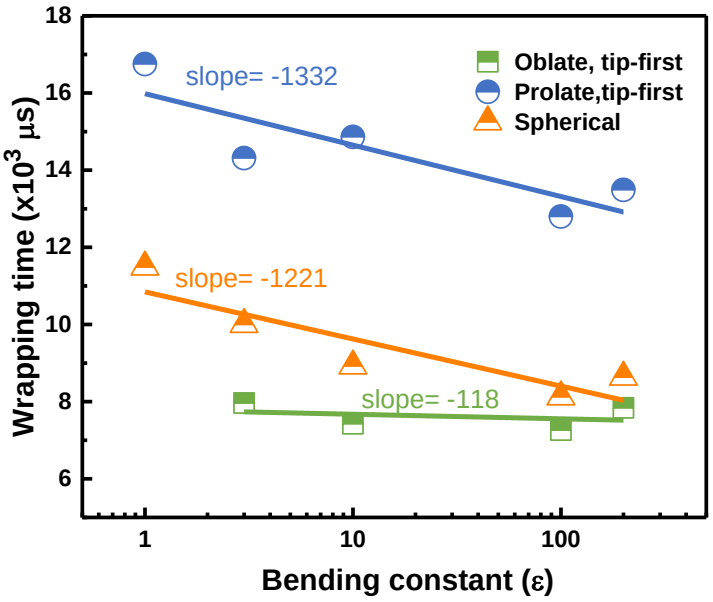

Figure 8: Wrapping time as a function of bending constant for oblate, prolate and spherical NPs.

To understand the interplay between the geometry and elasticity of NPs on their mem-

brane wrapping efficiency, we systematically study spherical, oblate and prolate NPs with a series of bending constants, ranging from $k_{\text{bend}} = 1\epsilon$ to $k_{\text{bend}} = 200\epsilon$. The wrapping time of these NPs is plotted against the bending constant k_{bend} for different NP geometries in Fig.8. Here the tip-first entry mode is adopted for non-spherical NPs. There are three interesting phenomena we can learn from Fig.8: (1) under the same bending constant, NP geometry plays a significant role. The membrane wrapping efficiency for different geometries is ranked as: oblate NPs > spherical NPs > prolate NPs; (2) under the same geometry, the wrapping time of NPs decreases with the bending constant increases. Furthermore, the wrapping time follows a scaling law against the bending constant. Interestingly, a similar scaling relation between the bending rigidity and cellular uptake efficiency is found for liposomes in experiments;[28] (3) for the scaling relation, the slope for oblate NPs is much smaller than that for spherical and prolate NPs. This indicates that the oblate shape is the least sensitive geometry to the bending constant change. In correspondence with these interesting results, the analyses about the contact edge length and energy barrier are given in Fig. S9 of Supporting Information. Under the same bending constant, the oblate NPs have the largest contact edge lengths, followed by spherical and prolate NPs. This large contact edge length for oblate NP makes oblate shape the most efficient geometry during membrane wrapping, as being observed in experiments.[68] Furthermore, under the same geometry, NPs with different bending constants have similar contact edge lengths. The energy barrier of NPs with the same geometry decreases as bending constant increases, leading to the scaling law between the bending constant and membrane wrapping time. Moreover, because of the significantly large contact edge length, soft oblate NPs have a high receptor recruiting speed to bind extra receptors for overcoming the increased energy barrier. Therefore, the oblate NPs are less sensitive to the variation of the bending constant.

For non-spherical NPs, due to their anisotropic properties, the initial entry angle of both oblate and prolate NPs affects their contact edge lengths and energy barriers.[16,21,23,24] To explore the influence of entry angle, we further study the membrane wrapping process of

oblate and prolate NPs with their minor and major axes parallel to the membrane plane, respectively. We call this entry scenario as the side-first entry mode. Interestingly, with the side-first entry mode, the wrapping efficiency of NPs with the same bending constant is ranked as: prolate > spherical > oblate. This ranking sequence is totally reversed compared to the non-spherical NPs with tip-first entry mode. Additionally, we investigate the membrane wrapping process of soft disc-like, rod-like and cubic NPs, due to their wide applications.[69–71] It is interesting to find that NPs of the same geometric category (one-dimensional shape: rod-like and prolate NPs; two-dimensional shape: disc-like and oblate NPs; three-dimensional shape: cubic and spherical NPs) share a similar membrane wrapping pathway and wrapping efficiency. Please refer to the Supporting Information for the effect of the entry angle and other non-spherical NPs.

Discussion

Larger receptor diffusion flux leads to more efficient membrane wrapping. Our simulation results provide clear evidence that the membrane wrapping efficiency (or wrapping rate) is a result of competition between the receptor diffusion kinetics and thermodynamic driving force. The receptor diffusion kinetics, referring to the kinetics of recruitment of receptors to the binding site, are related to the receptor diffusion flux and contact edge length. The thermodynamic driving force, representing the amount of free energy required to drive the NPs into the cell, is determined by energy barriers during membrane wrapping of NPs. The receptor diffusion flux and individual ligand-receptor binding strength are kept the same for all the simulations above. To further confirm our conclusion, we have performed additional simulations to understand the influence of receptor diffusion flux on the membrane wrapping efficiency of a rigid spherical NP with radius $R = 75$ nm. The receptor diffusion flux is determined by the receptor density gradient according to the Fick's first law. Note that the receptor density gradient is affected by the receptor density, due to the existence of the receptor depletion region in the near vicinity of the contact region

between the NP and membrane. Here we have systematically varied the receptor densities in the cell membrane. With the same spherical rigid NPs, the energy barrier at each wrapping ratio should be the same for all cases. As given in Fig. S13 in Supporting Information, at the same wrapping ratio of $f = 0.5$ and identical contact edge length, the slope of unbounded receptor density near the NP is dramatically increasing with the increment of the receptor density in the cell membrane. The corresponding receptor diffusion flux is almost linearly dependent on the receptor density. Therefore, the rigid NP should be more quickly wrapped by the membrane with a higher receptor density, which is observed in our simulations (Fig. S13B in Supporting Information). The relation between the wrapping time and membrane receptor density is given in Fig. S13D in Supporting Information. As the receptor density increases, the wrapping time dramatically decreases if the receptor density is smaller than $24.32 \times 10^{-4}/\text{nm}^2$, after which it levels off. The saturation of the wrapping time should be induced by the limited available unbounded ligands on the NP surface. At these high receptor densities, the influence of receptor diffusion kinetics on the wrapping efficiency has been eliminated, leading to a fast membrane wrapping of the rigid NP.

Different mechanical properties lead to conflicting results on efficiency of elastic NPs. In experiments, different elastic NPs have been synthesized, including liposomes, hybrid polymer-lipid NPs, layer-by-layer (LBL) capsules, and hydrogel NPs.[30] Modulation of their elasticity can be achieved by changing the phospholipid components (liposomes),[28,72] the materials of core (hybrid polymer-lipid NPs),[28] the layer number or thickness (LBL capsules)[34,73] and the cross-linking density (hydrogel NPs).[26,74] Conflicting results have been reported about the relation between cell internalization rate and particle elasticity. As shown in Table.1, we summarize experimental results about the influence of NPs' elasticity on their uptake by cancer cells. The softer lipid based NPs show lower internalization rates compared to their rigid counterparts. But the softer LBL capsules are more efficiently internalized. The hydrogel NPs give controversial results. Although the different experimental conditions might contribute to the conflicting results, our simulations might also provide a basic under-

standing behind these results. As we mentioned before, the membrane wrapping efficiency is determined by both contact edge length and energy barrier (or thermodynamic driving force). The softer NPs are proven to need to overcome a larger energy barrier because of their deformation in both theories and simulations. But the contact edge length difference between soft and rigid NPs is determined by their mechanical properties. Specifically, in theory, by removing the volume constraint and fixing the total area, the contact edge length of soft spherical NP in Yi and Gao's work is 20% larger than that of the rigid counterpart.[39] However, in our simulations, both the total volume and area of elastic NPs are controlled by the potential functions. Thus, the soft spherical NP has a similar contact edge as their rigid counterpart. Because of this difference, the soft NPs in Yi and Gao's work are faster than the rigid NPs to be fully wrapped.[39] While, in our simulations, soft NPs are less efficient. In experiments, the LBL capsules are hollow particles after removing the template. These particles can easily change their volumes during cellular uptake, leading to large contact lengths and high efficiencies of internalization.[34,73] On the other hand, for the lipid based NPs, due to the hydrophobicity of lipid bilayer, the interior water molecules are difficult to penetrate through the bilayer. Therefore, lipid based NPs can be considered as incompressible with constant volume, similar to the elastic NPs model in present study, which have lower cellular uptake efficiency for softer NPs.[28,72] Therefore, our works provide an insightful explanation for these conflicting experimental results.

Table 1: Experimental results about soft and rigid nanoparticles during cancer cell uptake.

Particle types	Shape	Size	Mechanical properties	Cell types	References
More efficient rigid NPs					
PEG* hygrogel	sphere	200 nm	**Bulk modulus:** 10 kPa–3000 kPa	41T cancer cells	[26]
PLGA*-lipid	sphere	100 nm/40 nm	**Young's modulus:** 800 MPa–1200 MPa	HeLa cells	[32,33]
PEGylated liposome	sphere	100 nm	**Bending rigidity:** $(2–14)\times10^{-19}$ J	HeLa cells	[28]
More efficient soft NPs					
HA* LbL capsule	sphere	2400 nm	**Stiffness:** 7.5 N/m–28 N/m	HeLa cells	[34]
DextS/PLArg* and PSS/PAH* LbL capsule	sphere	2500 nm	**Stiffness:** 0.25 N/m–10 N/m	HeLa cells	[35]
TA/PVPON LbL capsule	sphere/cube	2000 nm	**Young's modulus:** 4.3 MPa–10^4 MPa	SUM159 cancer cells	[75]
HEMA hygrogel	sphere	1100 nm	**Bulk modulus:** 15 kPa–156 kPa	HepG2 cells	[74]

*Abbreviations: PEG, poly-(ethylene glycol); HA, Hyaluronic acid; DextS, dextran sulfatesodium salt; PLArg, poly-l-arginine hydrochloride; PSS, poly(sodium 4-styrenesulfonate); PHA, poly(allylaminehydrochloride); TA/PVPON, tannic acid/poly(N-vinylpyrrolidone); HEMA, poly(2-hydroxyethyl methacrylate).

Conclusions

In this work, we have systematically investigated the receptor-mediated membrane wrapping process of elastic NPs with different sizes and shapes using CGMD simulations. The elasticity of NPs can be well controlled by the bending constant in our model. The membrane wrapping efficiency of elastic NPs is found to be governed by the receptor recruitment speed and free energy barriers. The receptor recruitment speed is determined by the receptor diffusion flux and contact edge length between the NP and membrane. The free energy barriers are mainly determined by the free energy changes of NPs and membrane. For spherical NPs, under the control of volume constraint, the contact edge lengths of soft and rigid NPs are found to be similar. Comparatively, soft spherical NPs have significantly higher energy barriers due to their ability to deform. Due to the increased energy barriers, soft spherical NPs need to recruit more receptors to provide the driving force for the membrane wrapping. Therefore, they are less efficiently fully wrapped than rigid ones. Furthermore, the free energy barrier for membrane wrapping of soft spherical NPs is increasing with their size under the same bending constant. As a result, the difference in the wrapping efficiency between soft and

rigid spherical NPs increases with their size.

For non-spherical oblate and prolate NPs, the rigid oblate NP needs to overcome a larger energy barrier compared to the rigid prolate NP. However, the oblate NP has a significantly large contact edge length which enables it to be fully wrapped faster than the prolate NP. More importantly, due to the prominent large contact edge length, the wrapping efficiency of the soft oblate NP is the least sensitive to the bending constant variation among the geometries of spherical, prolate and oblate shapes. Under the same bending constant, the wrapping efficiency is ranked as oblate NP $>$ spherical NP $>$ prolate NP for the tip-first entry mode. However, this ranking sequence is totally reversed when the entry angle of oblate and prolate NPs is changed to the side-first entry mode. It is worthy to note that according to our simulations, both the soft spherical and non-spherical NPs remain at a high energy state when fully wrapped and cannot return to their initial stress-free state. These simulations provide a way to understand the conflicting experimental results in terms of the influence of NP geometry and elasticity on their endocytosis efficiency. This work might provide a theoretical guidance for the NP design in targeted drug delivery.

Model and Methods

Lipid Membrane and Elastic Nanoparticles

In the one-bead lipid model, each lipid molecule is represented by a single spherical bead containing both the translational and rotational degrees of freedom. The interactive force between beads depends on their relative distance and orientation. This one-bead lipid model can correctly reproduce both dynamic and mechanical properties of the lipid membrane.[46,76,77] The membrane temperature is set to $T = 0.18\epsilon/k_{\mathrm{B}}$ during the membrane wrapping process, at which the membrane maintains its fluid state.[46] In the elastic NP model, the beads on the NP shell locate on a set of evenly distributed vertex points $\underline{\mathrm{x}}_i$, $i \in 1, ..., N_{\mathrm{v}}$. These vertex points are connected by N_{s} edges, forming N_{t} triangles on the shell. The

elasticity of NP can be controlled by the area V_{area}, volume V_{volume}, in-plane $V_{\text{in-plane}}$ and bending V_{bending} potentials. The total potential energy of an elastic NP is defined as

$$V(\underline{\mathrm{x}}_i) = V_{\text{area}} + V_{\text{volume}} + V_{\text{in-plane}} + V_{\text{bending}}.$$

In our simulations, the elasticity of NP is controlled by tuning the bending constant k_{bend} in the potential V_{bending}. The bending constant k_{bend} is directly related to the macroscopic bending rigidity of an elastic NP based on Helfrich model.[53,54] For instance, the macroscopic bending rigidity κ_{b} of spherical elastic NPs can be expressed as[53] $\kappa_{\text{b}} = \sqrt{3}k_{\text{bend}}/2$. Therefore, with the bending constant $k_{\text{bend}} = 0.1\epsilon$–$200\epsilon$, their corresponding macroscopic bending rigidities are around $\kappa_{\text{b}} \approx 0.48\ k_{\text{B}}T$–$956\ k_{\text{B}}T$, which covers the range of bending rigidities for liquid disordered state liposome and solid ordered state PEGylated liposome.[28,72,78] To model NPs of different shapes, the initial configurations of elastic shells are constructed according to different geometrical functions. Particularly, the rod-like and disc-like NPs are built based on the function $[(x^2+y^2)/a^2]^3 + (z/b)^6 = 1$. The aspect ratio of them is defined as b/a. The cubic NPs are built based on the function $x^6+y^6+z^6 = a^6$. To obtain the stable NPs, the triangularization of vertex points on the defined surface is of great importance.[53,54] During the triangularization process, N_{v} vertex points are firstly randomly distributed on the surface, and each connected edge is assigned a spring force based on its current edge length. These spring constants all have the same value. These N_{v} points are then free to move on the defined surfaces until all the spring forces on all connected edges have the same spring force value. Using this method we can construct stress-free NPs of different shapes.[79] Please refer to the Supporting Information for more details about lipid and NP models.

Ligand-Receptor Interaction

The ligands are evenly distributed on the NP surface. Certain lipids in the membrane are initially randomly selected as receptors that can specifically interact with ligands on the NP

surface. Therefore, the diffusion constant of receptors has the same value as that of lipids. As the area of the cell membrane is much larger than that of the NP, the receptor density in the region of cell membrane far away from the NP is constant during the endocytosis. To capture this feature, the boundary of the membrane serves as a receptor reservoir. Particularly, if one receptor in the membrane is already bound to a ligand, a lipid near the boundary will be correspondingly changed into a receptor. In this way, we can reproduce the constant receptor density boundary condition in simulations as is adopted in theory.[41] In CGMD simulations, to study the membrane wrapping process of NPs, the specific ligand-receptor interaction is usually represented by pair-wise interactions.[49,67,80] Under the pair-wise interactions, ligands on NP surface could interact with multiple receptors simultaneously. This unreasonable multi-binding behavior could induce local aggregation of receptors and provide extremely large binding energy during the membrane wrapping process, which is inconsistent with the ligand-receptor binding in biological system. To avoid this problem, the ligand-receptor interaction in our CGMD simulations is modeled by a bond-like interaction. With this model, a ligand can only bind with one receptor in a planar membrane at one time. This ligand-receptor interaction is governed by the potential as $V_{\rm lr}(r) = 72\epsilon[(\frac{\sigma}{r})^{1.6} - (\frac{\sigma}{r})^{0.8}]$ at $r < r_{\rm clr}$, where $r_{\rm clr} = 15\sigma$ is the cutoff distance, beyond which the ligand-receptor bond will break. The average ligand-receptor binding strength is around 10ϵ or 50 $k_{\rm B}T$. This strength is within the range of ligand-receptor binding energy from literature.[81–83]

Simulation Protocol

In our simulations, the mass m for each bead is set to be unity value, and the time step is $\Delta t = 0.005\tau$ with $\tau = \sqrt{\epsilon/(m\sigma^2)}$. The membrane tension is controlled by regulating the xy in-plane pressure through a modified Berendsen method.[67,84] The velocity-verlet integration algorithm is adopted for the time integration. The Nose-Hoover thermostat is used to maintain the temperature of the lipid bilayer, which is suggested for the one-bead lipid model.[46] Considering the missing solvent degrees of freedom in the solvent free model, the temper-

ature of NPs is controlled using the Langevin thermostat and maintained at $0.001\epsilon/k_{\mathrm{B}}$ to rule out the possible influence of thermal fluctuation on the mechanical behaviors of elastic NPs. The physical length and time scales corresponding to our simulations could be obtained by comparing the membrane thickness and diffusion coefficient between computational and experimental values. The typical membrane thickness in experiments is about 5 nm.[85,86] As the thickness of the membrane in our simulations is around 2σ, we have the basic length unit $\sigma \approx 2.5$ nm. The typical diffusion coefficient of the lipid molecules in the membrane is about 5 $\mu\mathrm{m}^2/\mathrm{s}$[87] in experiments. By mapping the lateral diffusion coefficient of lipids $D = 0.2\sigma^2/\tau$ in CGMD simulations with the experimental value, the basic time unit in simulations is determined as $\tau = 0.25$ μs. All simulations are performed with LAMMPS.[88] Please refer to the Supporting Information for more details about the properties of the lipid membrane.

Acknowledgement

Z.S., H.Y. and Y.L. are grateful to support from the Department of Mechanical Engineering at University of Connecticut. Z.S. and H.Y. would like to thank the partial financial support from GE Fellowship for innovation. This research benefited in part from the computational resources and staff contributions provided for Booth Engineering Center for Advanced Technology (BECAT) at University of Connecticut. Part of this work used the Extreme Science and Engineering Discovery Environment (XSEDE), which is supported by National Science Foundation grant number ACI-1053575. X.Y. acknowledges support from the National Natural Science Foundation of China under Grant 11872005. We are grateful to Alessandro Fisher and William Baker for critical reading of the manuscript.

Supporting Information Available

Details of the computational models for lipid membrane and elastic NPs, computational methods and additional simulation results. This material is available free of charge *via* the

Internet at http://pubs.acs.org.

References

1. Albanese, A.; Tang, P. S.; Chan, W. C. The Effect of Nanoparticle Size, Shape, and Surface Chemistry on Biological Systems. *Annu. Rev. Biomed. Eng.* **2012**, *14*, 1–16.

2. Zhang, S.; Gao, H.; Bao, G. Physical Principles of Nanoparticle Cellular Endocytosis. *ACS Nano* **2015**, *9*, 8655–8671.

3. Ding, H.-M.; Ma, Y.-Q. Theoretical and Computational Investigations of Nanoparticle–Biomembrane Interactions in Cellular Delivery. *Small* **2015**, *11*, 1055–1071.

4. Wilhelm, S.; Tavares, A. J.; Dai, Q.; Ohta, S.; Audet, J.; Dvorak, H. F.; Chan, W. C. Analysis of Nanoparticle Delivery to Tumours. *Nat. Rev. Mater.* **2016**, *1*, 16014.

5. Rosenblum, D.; Joshi, N.; Tao, W.; Karp, J. M.; Peer, D. Progress and Challenges towards Targeted Delivery of Cancer Therapeutics. *Nat. Commun.* **2018**, *9*, 1410.

6. Barenholz, Y. C. Doxil®-The First FDA-Approved Nano-Drug: Lessons Learned. *J. Controlled Release* **2012**, *160*, 117–134.

7. Kinnear, C.; Moore, T. L.; Rodriguez-Lorenzo, L.; Rothen-Rutishauser, B.; Petri-Fink, A. Form Follows Function: Nanoparticle Shape and Its Implications for Nanomedicine. *Chem. Rev.* **2017**, *117*, 11476–11521.

8. Kol, N.; Shi, Y.; Tsvitov, M.; Barlam, D.; Shneck, R. Z.; Kay, M. S.; Rousso, I. A Stiffness Witch in Human Immunodeficiency Virus. *Biophys. J.* **2007**, *92*, 1777–1783.

9. Nanbo, A.; Imai, M.; Watanabe, S.; Noda, T.; Takahashi, K.; Neumann, G.; Halfmann, P.; Kawaoka, Y. Ebolavirus Is Internalized into Host Cells *via* Macropinocytosis in a Viral Glycoprotein-Dependent Manner. *PLoS Pathog.* **2010**, *6*, e1001121.

10. Doherty, G. J.; McMahon, H. T. Mechanisms of Endocytosis. *Annu. Rev. Biochem.* **2009**, *78*, 857–902.

11. Chou, L. Y.; Ming, K.; Chan, W. C. Strategies for the Intracellular Delivery of Nanoparticles. *Chem. Soc. Rev.* **2011**, *40*, 233–245.

12. Florez, L.; Herrmann, C.; Cramer, J. M.; Hauser, C. P.; Koynov, K.; Landfester, K.; Crespy, D.; Mailänder, V. How Shape Influences Uptake: Interactions of Anisotropic Polymer Nanoparticles and Human Mesenchymal Stem Cells. *Small* **2012**, *8*, 2222–2230.

13. Zhang, Y.; Tekobo, S.; Tu, Y.; Zhou, Q.; Jin, X.; Dergunov, S. A.; Pinkhassik, E.; Yan, B. Permission to Enter Cell by Shape: Nanodisk *vs* Nanosphere. *ACS Appl. Mater. Interfaces* **2012**, *4*, 4099–4105.

14. Sharma, G.; Valenta, D. T.; Altman, Y.; Harvey, S.; Xie, H.; Mitragotri, S.; Smith, J. W. Polymer Particle Shape Independently Influences Binding and Internalization by Macrophages. *J. Controlled Release* **2010**, *147*, 408–412.

15. Dasgupta, S.; Auth, T.; Gompper, G. Wrapping of Ellipsoidal Nano-Particles by Fluid Membranes. *Soft Matter* **2013**, *9*, 5473–5482.

16. Bahrami, A. H. Orientational Changes and Impaired Internalization of Ellipsoidal Nanoparticles by Vesicle Membranes. *Soft Matter* **2013**, *9*, 8642–8646.

17. Chen, L.; Xiao, S.; Zhu, H.; Wang, L.; Liang, H. Shape-Dependent Internalization Kinetics of Nanoparticles by Membranes. *Soft Matter* **2016**, *12*, 2632–2641.

18. Chen, L.; Li, X.; Zhang, Y.; Chen, T.; Xiao, S.; Liang, H. Morphological and Mechanical Determinants of Cellular Uptake of Deformable Nanoparticles. *Nanoscale* **2018**, *10*, 11969–11979.

19. Richards, D. M.; Endres, R. G. Target Shape Dependence in a Simple Model of Receptor-Mediated Endocytosis and Phagocytosis. *Proc. Natl. Acad. Sci. U.S.A.* **2016**, *113*, 6113–6118.

20. Li, Y.; Yue, T.; Yang, K.; Zhang, X. Molecular Modeling of the Relationship between Nanoparticle Shape Anisotropy and Endocytosis Kinetics. *Biomaterials* **2012**, *33*, 4965–4973.

21. Dasgupta, S.; Auth, T.; Gompper, G. Shape and Orientation Matter for the Cellular Uptake of Nonspherical Particles. *Nano Lett.* **2014**, *14*, 687–693.

22. Tang, H.; Zhang, H.; Ye, H.; Zheng, Y. Receptor-Mediated Endocytosis of Nanoparticles: Roles of Shapes, Orientations, and Rotations of Nanoparticles. *J. Phys. Chem. B* **2017**, *122*, 171–180.

23. Huang, C.; Zhang, Y.; Yuan, H.; Gao, H.; Zhang, S. Role of Nanoparticle Geometry in Endocytosis: Laying Down to Stand Up. *Nano Lett.* **2013**, *13*, 4546–4550.

24. Li, Y.; Kröger, M.; Liu, W. K. Shape Effect in Cellular Uptake of PEGylated Nanoparticles: Comparison between Sphere, Rod, Cube and Disk. *Nanoscale* **2015**, *7*, 16631–16646.

25. Palomba, R.; Palange, A. L.; Rizzuti, I. F.; Ferreira, M.; Cervadoro, A.; Barbato, M. G.; Canale, C.; Decuzzi, P. Modulating Phagocytic Cell Sequestration by Tailoring Nanoconstruct Softness. *ACS Nano* **2018**, *12*, 1433–1444.

26. Anselmo, A. C.; Zhang, M.; Kumar, S.; Vogus, D. R.; Menegatti, S.; Helgeson, M. E.; Mitragotri, S. Elasticity of Nanoparticles Influences Their Blood Circulation, Phagocytosis, Endocytosis, and Targeting. *ACS Nano* **2015**, *9*, 3169–3177.

27. Beningo, K. A.; Wang, Y.-l. Fc-Receptor-Mediated Phagocytosis Is Regulated by Mechanical Properties of the Target. *J. Cell Sci.* **2002**, *115*, 849–856.

28. Takechi-Haraya, Y.; Goda, Y.; Sakai-Kato, K. Control of Liposomal Penetration into Three-Dimensional Multicellular Tumor Spheroids by Modulating Liposomal Membrane Rigidity. *Mol. Pharmaceutics* **2017**, *14*, 2158–2165.

29. Yu, M.; Xu, L.; Tian, F.; Su, Q.; Zheng, N.; Yang, Y.; Wang, J.; Wang, A.; Zhu, C.; Guo, S.; Zhang, X.; Gan, Y.; Shi, X.; Gao, H. Rapid Transport of Deformation-Tuned Nanoparticles across Biological Hydrogels and Cellular Barriers. *Nat. Commun.* **2018**, *9*, 2607.

30. Anselmo, A. C.; Mitragotri, S. Impact of Particle Elasticity on Particle-Based Drug Delivery Systems. *Adv. Drug Delivery Rev.* **2017**, *108*, 51–67.

31. Di Francesco, M.; Primavera, R.; Romanelli, D.; Palomba, R.; Pereira, R. C.; Catelani, T.; Celia, C.; Di Marzio, L.; Fresta, M.; Di Mascolo, D.; Decuzzi, P. Hierarchical Microplates as Drug Depots with Controlled Geometry, Rigidity, and Therapeutic Efficacy. *ACS Appl. Mater. Interfaces* **2018**, *10*, 9280–9289.

32. Zhang, L.; Feng, Q.; Wang, J.; Zhang, S.; Ding, B.; Wei, Y.; Dong, M.; Ryu, J.-Y.; Yoon, T.-Y.; Shi, X.; Sun, J.; Jiang, X. Microfluidic Synthesis of Hybrid Nanoparticles with Controlled Lipid Layers: Understanding Flexibility-Regulated Cell–Nanoparticle Interaction. *ACS Nano* **2015**, *9*, 9912–9921.

33. Sun, J.; Zhang, L.; Wang, J.; Feng, Q.; Liu, D.; Yin, Q.; Xu, D.; Wei, Y.; Ding, B.; Shi, X.; Jiang, X. Tunable Rigidity of (Polymeric Core)–(Lipid Shell) Nanoparticles for Regulated Cellular Uptake. *Adv. Mater.* **2015**, *27*, 1402–1407.

34. Sun, H.; Wong, E. H.; Yan, Y.; Cui, J.; Dai, Q.; Guo, J.; Qiao, G. G.; Caruso, F. The Role of Capsule Stiffness on Cellular Processing. *Chem. Sci.* **2015**, *6*, 3505–3514.

35. Hartmann, R.; Weidenbach, M.; Neubauer, M.; Fery, A.; Parak, W. J. Stiffness-Dependent *in Vitro* Uptake and Lysosomal Acidification of Colloidal Particles. *Angew. Chem. Int. Ed.* **2015**, *54*, 1365–1368.

36. Yi, X.; Shi, X.; Gao, H. Cellular Uptake of Elastic Nanoparticles. *Phys. Rev. Lett.* **2011**, *107*, 098101.

37. Yi, X.; Gao, H. Cell Membrane Wrapping of a Spherical Thin Elastic Shell. *Soft Matter* **2015**, *11*, 1107–1115.

38. Li, Y.; Zhang, X.; Cao, D. Nanoparticle Hardness Controls the Internalization Pathway for Drug Delivery. *Nanoscale* **2015**, *7*, 2758–2769.

39. Yi, X.; Gao, H. Kinetics of Receptor-Mediated Endocytosis of Elastic Nanoparticles. *Nanoscale* **2017**, *9*, 454–463.

40. Chithrani, B. D.; Chan, W. C. Elucidating the Mechanism of Cellular Uptake and Removal of Protein-Coated Gold Nanoparticles of Different Sizes and Shapes. *Nano Lett.* **2007**, *7*, 1542–1550.

41. Gao, H.; Shi, W.; Freund, L. B. Mechanics of Receptor-Mediated Endocytosis. *Proc. Natl. Acad. Sci. U.S.A.* **2005**, *102*, 9469–9474.

42. Jiang, W.; Kim, B. Y.; Rutka, J. T.; Chan, W. C. Nanoparticle-Mediated Cellular Response Is Size-Dependent. *Nat. Nanotechnol.* **2008**, *3*, 145–150.

43. Zhang, S.; Li, J.; Lykotrafitis, G.; Bao, G.; Suresh, S. Size-Dependent Endocytosis of Nanoparticles. *Adv. Mater.* **2009**, *21*, 419–424.

44. Chen, Y.; Munteanu, A. C.; Huang, Y.-F.; Phillips, J.; Zhu, Z.; Mavros, M.; Tan, W. Mapping Receptor Density on Live Cells by Using Fluorescence Correlation Spectroscopy. *Chem. Eur. J.* **2009**, *15*, 5327–5336.

45. Elias, D. R.; Poloukhtine, A.; Popik, V.; Tsourkas, A. Effect of Ligand Density, Receptor Density, and Nanoparticle Size on Cell Targeting. *Nanomed. Nanotechnol. Biol. Med.* **2013**, *9*, 194–201.

46. Yuan, H.; Huang, C.; Li, J.; Lykotrafitis, G.; Zhang, S. One-Particle-Thick, Solvent-Free, Coarse-Grained Model for Biological and Biomimetic Fluid Membranes. *Phys. Rev. E* **2010**, *82*, 011905.

47. Agudo-Canalejo, J.; Lipowsky, R. Critical Particle Sizes for the Engulfment of Nanoparticles by Membranes and Vesicles with Bilayer Asymmetry. *ACS Nano* **2015**, *9*, 3704–3720.

48. Fuchs, H.; Lücken, U.; Tauber, R.; Engel, A.; Geßner, R. Structural Model of Phospholipid-Reconstituted Human Transferrin Receptor Derived by Electron Microscopy. *Structure* **1998**, *6*, 1235–1243.

49. Vácha, R.; Martinez-Veracoechea, F. J.; Frenkel, D. Receptor-Mediated Endocytosis of Nanoparticles of Various Shapes. *Nano Lett.* **2011**, *11*, 5391–5395.

50. Vácha, R.; Martinez-Veracoechea, F. J.; Frenkel, D. Intracellular Release of Endocytosed Nanoparticles upon a Change of Ligand–Receptor Interaction. *ACS Nano* **2012**, *6*, 10598–10605.

51. Shen, Z.; Ye, H.; Li, Y. Understanding Receptor-Mediated Endocytosis of Elastic Nanoparticles through Coarse Grained Molecular Dynamic Simulation. *Phys. Chem. Chem. Phys.* **2018**, *20*, 16372–16385.

52. Curk, T.; Wirnsberger, P.; Dobnikar, J.; Frenkel, D.; Saric, A. Controlling Cargo Trafficking in Multicomponent Membranes. *Nano Lett.* **2018**, *18*, 5350–5356.

53. Fedosov, D. A.; Caswell, B.; Karniadakis, G. E. A Multiscale Red Blood Cell Model with Accurate Mechanics, Rheology, and Dynamics. *Biophys. J.* **2010**, *98*, 2215–2225.

54. Fedosov, D. A. Multiscale Modeling of Blood Flow and Soft Matter. PhD Thesis, Brown University, Providence, RI, 2010.

55. Ye, H.; Shen, Z.; Li, Y. Computational Modeling of Magnetic Particle Margination within Blood Flow through LAMMPS. *Comput. Mech.* **2018**, *62*, 457–476.

56. Liu, J.; Weller, G. E.; Zern, B.; Ayyaswamy, P. S.; Eckmann, D. M.; Muzykantov, V. R.; Radhakrishnan, R. Computational Model for Nanocarrier Binding to Endothelium Validated Using *in Vivo*, *in Vitro*, and Atomic Force Microscopy Experiments. *Proc. Natl. Acad. Sci. U.S.A.* **2010**, *107*, 16530–16535.

57. Bradley, R.; Radhakrishnan, R. Coarse-Grained Models for Protein-Cell Membrane Interactions. *Polymers* **2013**, *5*, 890–936.

58. Seifert, U.; Lipowsky, R. Adhesion of Vesicles. *Phys. Rev. A* **1990**, *42*, 4768–4771.

59. Long, R.; Hui, C.-Y.; Jagota, A.; Bykhovskaia, M. Adhesion Energy Can Regulate Vesicle Fusion and Stabilize Partially Fused States. *J. Royal Soc. Interface* **2012**, *9*, 1555–1567.

60. Yi, X.; Shi, X.; Gao, H. A Universal Law for Cell Uptake of One-Dimensional Nanomaterials. *Nano Lett.* **2014**, *14*, 1049–1055.

61. Deserno, M. Elastic Deformation of a Fluid Membrane upon Colloid Binding. *Phys. Rev. E* **2004**, *69*, 031903.

62. Liang, J.; Chen, P.; Dong, B.; Huang, Z.; Zhao, K.; Yan, L.-T. Ligand–Receptor Interaction-Mediated Transmembrane Transport of Dendrimer-Like Soft Nanoparticles: Mechanisms and Complicated Diffusive Dynamics. *Biomacromolecules* **2016**, *17*, 1834–1844.

63. Mao, J.; Guo, R.; Yan, L.-T. Simulation and Analysis of Cellular Internalization Pathways and Membrane Perturbation for Graphene Nanosheets. *Biomaterials* **2014**, *35*, 6069–6077.

64. Shen, Z.; Ye, H.; Kröger, M.; Li, Y. Aggregation of Polyethylene Glycol Polymers Suppresses Receptor-Mediated Endocytosis of PEGylated Liposomes. *Nanoscale* **2018**, *10*, 4545–4560.

65. Ruiz-Herrero, T.; Velasco, E.; Hagan, M. F. Mechanisms of Budding of Nanoscale Particles through Lipid Bilayers. *J. Phys. Chem. B* **2012**, *116*, 9595–9603.

66. Deserno, M.; Gelbart, W. M. Adhesion and Wrapping in Colloid-Vesicle Complexes. *J. Phys. Chem. B* **2002**, *106*, 5543–5552.

67. Shi, X.; von Dem Bussche, A.; Hurt, R. H.; Kane, A. B.; Gao, H. Cell Entry of One-Dimensional Nanomaterials Occurs by Tip Recognition and Rotation. *Nat. Nanotechnol.* **2011**, *6*, 714–719.

68. Agarwal, R.; Singh, V.; Jurney, P.; Shi, L.; Sreenivasan, S.; Roy, K. Mammalian Cells Preferentially Internalize Hydrogel Nanodiscs over Nanorods and Use Shape-Specific Uptake Mechanisms. *Proc. Natl. Acad. Sci. U.S.A.* **2013**, *110*, 17247–17252.

69. Xia, X.; Yang, M.; Wang, Y.; Zheng, Y.; Li, Q.; Chen, J.; Xia, Y. Quantifying the Coverage Density of Poly (Ethylene Glycol) Chains on the Surface of Gold Nanostructures. *ACS Nano* **2011**, *6*, 512–522.

70. Tang, B.; Xu, S.; An, J.; Zhao, B.; Xu, W.; Lombardi, J. R. Kinetic Effects of Halide Ions on the Morphological Evolution of Silver Nanoplates. *Phys. Chem. Chem. Phys.* **2009**, *11*, 10286–10292.

71. Huang, X.; Li, L.; Liu, T.; Hao, N.; Liu, H.; Chen, D.; Tang, F. The Shape Effect of Mesoporous Silica Nanoparticles on Biodistribution, Clearance, and Biocompatibility *in Vivo*. *ACS Nano* **2011**, *5*, 5390–5399.

72. Takechi-Haraya, Y.; Sakai-Kato, K.; Abe, Y.; Kawanishi, T.; Okuda, H.; Goda, Y.

Atomic Force Microscopic Analysis of the Effect of Lipid Composition on Liposome Membrane Rigidity. *Langmuir* **2016**, *32*, 6074–6082.

73. Dubreuil, F.; Elsner, N.; Fery, A. Elastic Properties of Polyelectrolyte Capsules Studied by Atomic-Force Microscopy and RICM. *Eur. Phys. J. E* **2003**, *12*, 215–221.

74. Liu, W.; Zhou, X.; Mao, Z.; Yu, D.; Wang, B.; Gao, C. Uptake of Hydrogel Particles with Different Stiffness and Its Influence on HepG2 Cell Functions. *Soft Matter* **2012**, *8*, 9235–9245.

75. Alexander, J. F.; Kozlovskaya, V.; Chen, J.; Kuncewicz, T.; Kharlampieva, E.; Godin, B. Cubical Shape Enhances the Interaction of Layer-By-Layer Polymeric Particles with Breast Cancer Cells. *Adv. Healthcare Mater.* **2015**, *4*, 2657–2666.

76. Fu, S.-P.; Peng, Z.; Yuan, H.; Kfoury, R.; Young, Y.-N. Lennard-Jones Type Pair-Potential Method for Coarse-Grained Lipid Bilayer Membrane Simulations in LAMMPS. *Comput. Phys. Commun.* **2017**, *210*, 193–203.

77. Yuan, H.; Huang, C.; Zhang, S. Dynamic Shape Transformations of Fluid Vesicles. *Soft Matter* **2010**, *6*, 4571–4579.

78. Gracià, R. S.; Bezlyepkina, N.; Knorr, R. L.; Lipowsky, R.; Dimova, R. Effect of Cholesterol on the Rigidity of Saturated and Unsaturated Membranes: Fluctuation and Electrodeformation Analysis of Giant Vesicles. *Soft Matter* **2010**, *6*, 1472–1482.

79. Ye, H.; Shen, Z.; Li, Y. Cell Stiffness Governs Its Adhesion Dynamics on Substrate under Shear Flow. *IEEE Trans. Nanotechnol.* **2018**, *17*, 407–411.

80. Shen, Z.; Loe, D. T.; Awino, J. K.; Kröger, M.; Rouge, J. L.; Li, Y. Self-Assembly of Core-Polyethylene Glycol-Lipid Shell (CPLS) Nanoparticles and Their Potential as Drug Delivery Vehicles. *Nanoscale* **2016**, *8*, 14821–14835.

81. Puvanendrampillai, D.; Mitchell, J. B. Protein Ligand Database (PLD): Additional Understanding of the Nature and Specificity of Protein–Ligand Complexes. *Bioinformatics* **2003**, *19*, 1856–1857.

82. Longo, G. S.; Thompson, D. H.; Szleifer, I. Ligand-Receptor Interactions between Surfaces: The Role of Binary Polymer Spacers. *Langmuir* **2008**, *24*, 10324–10333.

83. Chen, X.; Ji, Z. L.; Zhi, D.; Chen, Y. Z. CLiBE: A Database of Computed Ligand Binding Energy for Ligand-Receptor Complexes. *Comput. Chem.* **2002**, *26*, 661–666.

84. Guan, Z.; Wang, L.; Lin, J. Interaction Pathways between Plasma Membrane and Block Copolymer Micelles. *Biomacromolecules* **2017**, *18*, 797–807.

85. Kučerka, N.; Liu, Y.; Chu, N.; Petrache, H. I.; Tristram-Nagle, S.; Nagle, J. F. Structure of Fully Hydrated Fluid Phase DMPC and DLPC Lipid Bilayers Using X-ray Scattering from Oriented Multilamellar Arrays and from Unilamellar Vesicles. *Biophys. J.* **2005**, *88*, 2626–2637.

86. Discher, D. E.; Eisenberg, A. Polymer Vesicles. *Science* **2002**, *297*, 967–973.

87. Orädd, G.; Lindblom, G.; Westerman, P. W. Lateral Diffusion of Cholesterol and Dimyristoylphosphatidylcholine in a Lipid Bilayer Measured by Pulsed Field Gradient Nmr Spectroscopy. *Biophys. J.* **2002**, *83*, 2702–2704.

88. Plimpton, S. Fast Parallel Algorithms for Short-Range Molecular Dynamics. *J. Comput. Phys.* **1995**, *117*, 1–19.

Graphical TOC Entry